Custom-built electrostatics and supplementary bonding in the design of reinforced Collagen-g-P(methyl methacrylate-co-Ethyl Acrylate)/ nylon 66 core-shell fibers

Custom-built electrostatics and supplementary bonding in the design of reinforced Collagen-g-P(methyl methacrylate-co-Ethyl Acrylate)/ Nylon 66 core-shell fibers

Zahra Bazrafshan, George K. Stylios

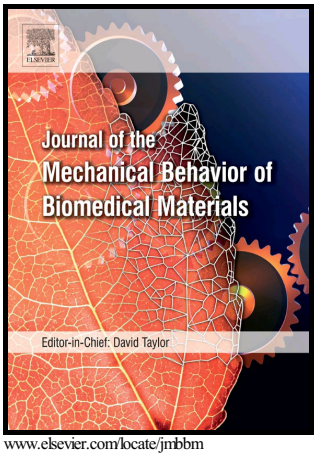

www.elsevier.com/locate/jmbbm

PII: S1751-6161(18)30154-1
DOI: https://doi.org/10.1016/j.jmbbm.2018.07.002
Reference: JMBBM2870

To appear in: *Journal of the Mechanical Behavior of Biomedical Materials*

Received date: 14 February 2018
Revised date: 24 April 2018
Accepted date: 1 July 2018

Cite this article as: Zahra Bazrafshan and George K. Stylios, Custom-built electrostatics and supplementary bonding in the design of reinforced Collagen-g-P(methyl methacrylate-co-Ethyl Acrylate)/ Nylon 66 core-shell fibers, *Journal of the Mechanical Behavior of Biomedical Materials,* https://doi.org/10.1016/j.jmbbm.2018.07.002

Title:

Custom-built electrostatics and supplementary bonding in the design of reinforced Collagen-g-P(methyl methacrylate-co-Ethyl Acrylate)/ Nylon 66 core-shell fibers

Zahra Bazrafshan (First Author), George K. Stylios (Co-Author).

Author information

1

Research Institute for Flexible Materials, School of Textiles and Design, Heriot-Watt University, Galashiels TD1 3HF, UK. zb4@hw.ac.uk, zahrabazrafshan@yahoo.com.

2

Research Institute for Flexible Materials, School of Textiles and Design, Heriot-Watt University, Galashiels TD1 3HF, UK. g.stylios@hw.ac.uk.

Abstract

In this study, Acid Soluble Collagen-g-P(methyl methacrylate-co-ethyl acrylate) (CME) was synthesized to take advantage of the flexibility of the resulted branched polymer chains and the high density of their chain entanglement. The coaxial electrospinning technique was applied to study the effect of electrically and structurally varied materials on fiber formation and fiber morphology when CME and Nylon 66 were electrospun as core and shell respectively. By tailoring the electrostatic field, different fiber content was achieved. The effect of chain orientation and intermolecular forces between the polymeric chains was investigated in the formed fibers by measuring thermal and mechanical properties, hydration degree and degradability. This approach to *in situ* fiber formation is not restricted to biomedical, but has potential end-uses in a variety of multi-functional applications.

Keywords: Branched Polymer, Coaxial Electrospinning, Collagen, Hydrogen Bonding, Degradability, Chain orientation, linear Polymer, Dipole polarization

1. Introduction

Development of engineered materials with tailored properties e.g. thermal or mechanical for specific applications is a promising field in material science(Correia et al., 2016; Pezzoli et al., 2017). In biomaterials and particularly in natural-based polymers such as collagen, it is essential to modify their properties to desired conditions(Averous and Pollet, 2011; Bledzki and Gassan, 1999; Li et al., 2002). There are several methods for modifying natural-based polymers such as grafting, blending and curing and associated derivations (Bhattacharya and Misra, 2004; Kaith et al., 2009).

Collagen is a natural polymer with excellent biocompatibility that cannot be applied freely due to its inherent drawbacks such as poor mechanical properties and fast degradability when their protein chains are switched to random coil conformation (Li et al., 2005; Li et al., 2013; Poormasjedi-Meibod et al., 2016; Yang et al., 2008; Zeugolis et al., 2008). Most researches on collagen, are focused on reducing its hydrophilic behavior whilst benefiting from its controllable biodegradation(Abbah et al., 2015). Therefore, the main uses of collagen based materials have been found in drug delivery, filtration, tissue scaffolds and wound dressing by mostly applying crosslinking methods (Li et al., 2005; Mariod and Adam, 2013; Matthews et al., 2002). These methods are basically performed as post treatment on produced collagen based materials, e.g., films and fibrous assemblies. However, it is believed that

prior to reaching the post treatment step, collagen polymer chains lose their properties, e.g., thermal and mechanical, to conform to severe process conditions (Yang et al., 2008; Zeugolis et al., 2008).

The lost properties are mostly due to the fast denaturation of hydrolyzing chain of the collagen in acidic solvents. Even though high concentration solutions(Cross et al., 2010) and applying salt crystals(Zeugolis et al., 2009) can slightly reduce the effect of the acid denaturation on electrostatic repulsion resulting from the positive charge build-up, the complete elimination of ions before crosslinking can be problematic for desired morphologies. However, collagen can be modified by graft polymerization to reduce its superhydrophilicity and to control biodegradation (Bhuiyan et al., 2015; Fujisawa and Kadoma, 2010; Solouk et al., 2015). This methodology can be applied to collagen and its derivations before processing. In this approach, different vinyl group monomers with varied physiochemical properties can be branched over the protein chain.

Hence, to control the degradation rate and hydrophilicity of the collagen chains, the achieved branched copolymer can have new behaviors different from the origin (e.g., rheological, thermal, electrical)(Bazrafshan and Stylios, 2017). This presents new challenges and opportunities. More specifically, in fiber formation, collagen based copolymers with branched structure require to be spun under specific conditions to prevent rayleigh instability of high entanglements. This issue can be easily addressed by the electrospinning method (McKee et al., 2004; Song et al., 2017; Wood-Adams et al., 2000) when the branched copolymers are spun in low concentrations.

When it comes to mechanical reinforcement of collagen based materials, blending with (semi-)synthetics is mainly recommended in traditional fiber formation methodologies (Mercader et al., 2010; Satyanarayana et al., 2009). Even though, this method is not as simple as it seems; phase segregations and viscosity changes are the simple examples of incompatible (co)polymeric fluids. This issue is due to different properties such as electrical and structural that can significantly limit the application(Krissinel and Henrick, 2007) of collagen based materials in fibrous assemblies. Interestingly, with coaxial electrospinning, working fluids with a wide variety of properties can be tuned for creating core-shell nanostructures(Bhardwaj and Kundu, 2010) simply with pure solvents(Wang et al., 2017; Yu et al., 2017). However, the performance of this technique in large scale fiber formation and fiber collection is still in its infancy.

In this work, we investigate a new approach to form hierarchical, robust fibrous electrospun collagen based materials which has a promising potential to conjugate with a variety of nanostructure materials from minerals to medicines. This is a novel attempt for spinning hydrophilic collagen based polymers whilst improving their mechanical properties. This is achieved by benefitting from different performance of the participated materials by supplementary bonding. P(Methyl Methacrylate-co-Ethyl Acrylate) was grafted onto the acid soluble collagen (ASC). The ASC-g-P(MMA-co-EA) was coelectrospun wherein Nylon 66 was used as a core fluid. End uses can consequently take the advantage of *in situ* fiber formation of the natural segment of collagen in the shell and mechanical strength of the core as a composite in the shape of a fiber to fabric, as shown in Fig. 1. We show that different polymeric content in core and shell can demonstrate improved properties by means of tunable electrical field. The mechanical, chemical, thermal and swelling behaviors of the core shell composite fiber structure were established. This work can be considered as a promising alternative to existing fibrous assemblies intending to exploit the advantages of chain flexibility in hydrophilic reinforced copolymers.

2. Materials and methods

2.1. *Materials*

Collagen from cow skin was provided by Devro Company Inc., UK. Methyl methacrylate (MMA, 99%, Alfa Aesar), Ethyl Acrylate (EA, 99%, Alfa Aesar) were used as process monomers and were passed through a column of 5% sodium hydroxide acquis solution to remove any inhibitor existed in them. Benzoyl peroxide (BPO,97%, Alfa Aesar) was used as initiator and recrystallized in Acetone before applying. Distilled water was used as a medium in the polymerization process. Acetic acid (AA, 99.7%, Alfa Aesar), Formic Acid (FA, 97 %, Alfa Aesar), Nylon 66 (N66, 262.35 g.mol^{-1}, Sigma Aldrich) and Methanol (MeOH, 99.9%, Alfa Aesar) were applied as received. D&C Red 28 (Rdye, Acid Red 92, Clariant, Switzerland) and Sanolin Tartrazine X90 (Ydye, Acid Yellow 23) were utilized as tinted indicators to distinguish the core and shell components, respectively.

2.2. *Synthesis of ASC-g-P(MMA-co-EA)*

The procedure of the copolymer synthesis has been reported in detail in our previous work(Bazrafshan and Stylios, 2017). A typical graft polymerization procedure (See supplementary data, Fig1) was applied for synthesis of the branched ASC-g-P(MMA-co-EA (CME). Briefly, ASC (11 g) was prepared using collagen in 0.1 M of AA and water to reach pH of 3±1. The mixture was incubated for 5 h at 45 °C in a 250-ml triple necked round bottom flask and a stirrer bar was added. Subsequently, conventional free radical polymerization was used to synthesize the graft copolymers of MMA-co-EA onto ASC in water (80 ml).

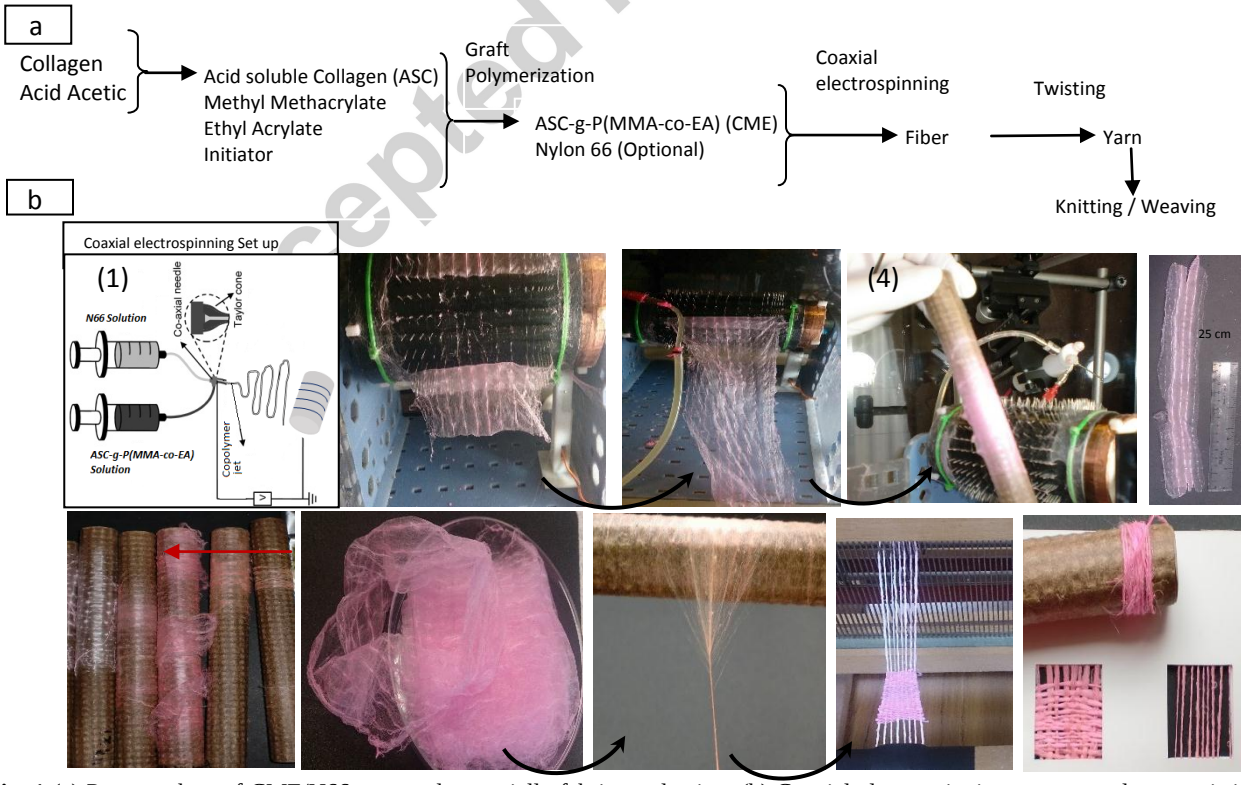

Fig. 1 (a) Process chart of CME/N66 yarn and potentially fabric production. (b) Coaxial electrospinning process and yarn twisting. (1) Coaxial electrospinning using rotating drum as collector. (2-5) Manually CME/N66 filaments were taken up around the nail drum (6) the color changing from pinkish yellow to yellowish pink by increasing the applied voltage that indicates the varied fiber in component. (7-10) The fibers were twisted into a yarn with clockwise twisting(S-twists) that is mechanically strong to be knitted /woven.

Table 1
Process parameters and observations

Solution [a]	Distance (cm)	Voltage (kV)	Flowrate (ml/h)	T (°C)	RH (%)	Observation
CME, 10wt/v%+ Ydye 0.1 wt% in FA	12	5-11	0.5	22±2	35±5	A nonwoven mat is formed in yellow color on the drum in
	12	12-20	1.5	22±2	35±5	a 5-minute, no solution dropping observed
N66,18wt/v% + Rdye 0.1t% in FA	12	5-12	0.5-1	22±2	35±5	Dropping, no tailor cone angle, no electrospun fiber is observed
	12	14-20	0.5-1	22±2	35±5	2d nano mat in the shade of light pink is achieved all over the drum in a 20-minute

Core solution [b]	Sheath solution	Distance (cm)	Voltage (kV)	Flowrate (mL/h)		T(°c)	RH(%)	Comments (Coaxial CME/N6)
				core	Sheath			
N6,25wt/v% + Rdye 0.1t% in FA	CME,10wt/v%+ 0.1 wt% in FA	Ydye 12	9.5-10	1	0.5	22±2	35±5	Occasionally droplet of N6 observed
		12	17-17.5	1	0.5	22±2	35±5	Chaotic CME polymer jet whipping in the air while the thin layer on 2d nonwoven mat forming on drum
		12	12-12.5	1	0.5	22±2	35±5	No droplet observed

a) The process parameters when they were electrospun separately
b) The coaxial electrospinning process parameters

Once the desired temperature of 80°C was achieved, BPO ($9.10*10^{-4}$ M) dissolved in Acetone and was gently added to the reaction vessel within 10 min as the initiator. MMA-co-EA ($109.83*10^{-4}$ M, 0.5% EA Content) were then introduced via a syringe in 30 min. The temperature and reaction time after adding the monomers were fixed to 80°C for 60 min. The reaction mixture was then added to excess amount of cool MeOH for complete precipitation. Then the solution was filtered and dried in a vacuum oven in 25°C until a constant weight was obtained. To remove any ungrafted ASC, the grafted copolymer was treated in boiling water, and then was washed with excess acetone to remove the associated P(MMA-co-EA). The resulted copolymer (CME) was dried in a vacuum oven at room temperature until a constant weight was achieved.

2.3. Preparation of spinning solutions and coaxial electrospinning

FA was used as the solvent for both solutions of the core and the shell fluids. The core solution consisted of N66 and Rdye in FA under stirring for 4 h at 70°C. The shell solution made up of CME and Ydye dissolved in FA in 8 h at room temperature. To follow the electrospinning procedure, two distinguished dye shades with no overlay in color spectrum were used (Red and Yellow). The solutions were loaded into a 10-mL and a 5-mL syringe as core and shell components, respectively. Detailed sample descriptions, including electrospinning parameters, are shown in Table 1. A positively charged coaxial needle (gauge 20 & 26) was used as spinneret. A rotating drum with nails was applied as collector with a fixed rotation speed (423 rpm) in all experiments. The Spreybase® electrospinning system was used.

2.4. Characterizations

To study the size and morphology of the electrospun fibers, Scanning Electron Microscopy (SEM, Hitachi S-4300) was used at an operating voltage of 3 kV. The electrospun fibers were coated with a gold thin film before SEM imaging to ensure higher conductivity. The mean fiber diameter and the uniformity of the fibers (standard deviation value), were estimated statistically by using ImageJ software from SEM micrographs. To determine the fiber alignment, Fast Fourier transform (FFT) was performed using ImageJ on representative images. FFT analysis created a pixel intensity image based on the frequency and direction of the fibers. The reverse FFT data was plotted over 180° from the radial summation of pixel intensity from the FFT analysis. Then mechanical properties of the produced fibers in the yarn bundle were determined by using an Instron Tester (3345 series) for the twisted yarns (n=5) using the BS-EN-ISO 2062:2009 standard. The gauge length was set at 50 mm for all specimens and a rate of extension of 10 mm/min under standard atmospheric conditions for testing. The structure of the electrospun fibers were considered by Fourier Transform Infrared Spectroscopy (FT-IR, Thermo Nicolet Avatar 370 DTGS) at room temperature without dyes. To prepare the disk, the fibers (1 w%) were prepared in KBr. Thermal analysis of fibers was performed by Differential Scanning Calorimeter (DSC, Mettler DSC 12E). Temperature ranges from 23°C up to 300°C and vice versa for cooling scans with a heating/cooling rate of 10°C min-1 in nitrogen atmosphere was performed. A 3 minute- time remaining at 300℃ was applied to erase the history of the thermal behavior of samples (7mg) for evaluating changes during the cooling scans. Endotherms were represented with upward curves in the scans. A heat of fusion of 255.8 $J.g^{-1}$ (ΔHm°) was presumed for 100 % crystalline N66, in crystallinity measurements. The degree of crystallinity (%) of the samples were obtained from:

$$C(\%) = \frac{[\Delta Hm - \Delta Hc]}{\Delta Hm^{\circ}} * 100$$

where $(\Delta Hm - \Delta Hc)$ was the measured heat of fusion(Chen et al., 2008).

The water contact angles of different fiber samples were measured by a contact angel analyzer (OneAttention v. 2.3, Boilin Scientific, n=5). Hydration degrees (water absorption) were studied by weighing the fiber samples before and after immersion in

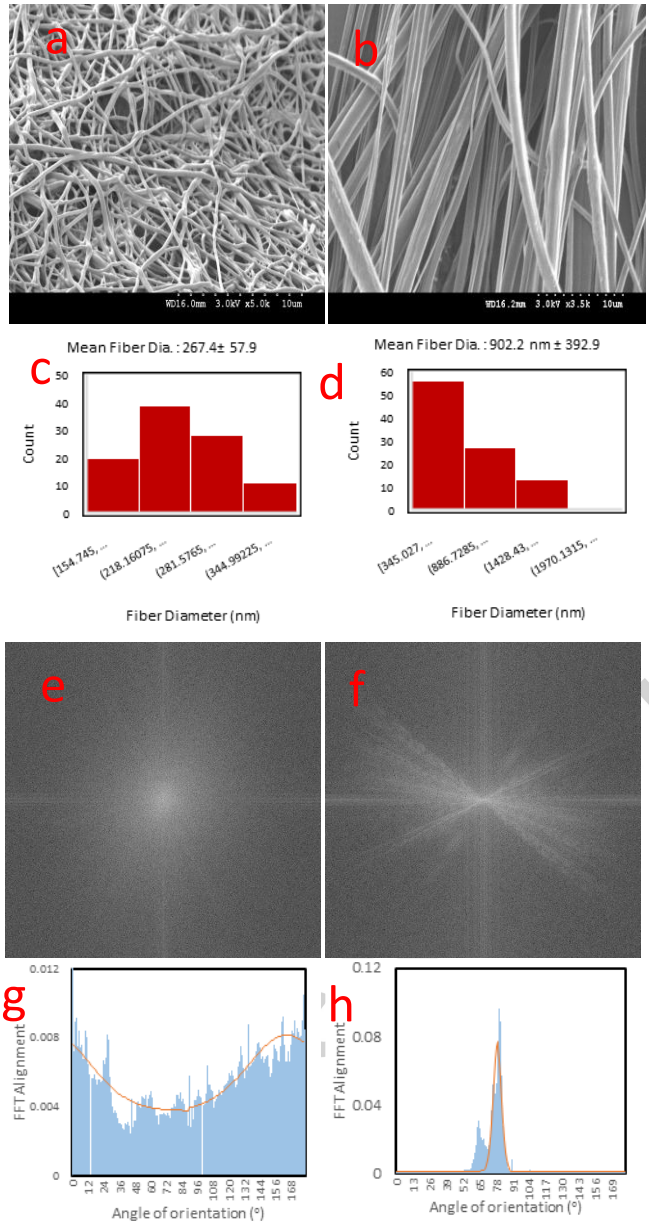

Figure 2 Investigation of morphology and alignment of the electrospun Nylon 66 nanofibers (a, c, e, g) and ASC-g-P(MMA-co-EA) nanofibers (b, d, f, h). (a, b) SEM images of the Nylon 66 and ASC-g-P(MMA-co-EA) nanofibers collected by a rotating drum with constant rotary speed of 423 rpm, using a typical electrospinning setup and (c, d) fiber diameter frequency plots; (e, f) Image J Raw output of the 2-D FFT alignment analysis of electrospun fibers corresponding to SEM images in (a, b); (g, h) the directionality histogram reporting 2D-FFT alignment based on peak shape and the relative principle axis of orientation for the fibers.

distilled water for 12 hours. Excess water was removed from the samples by gently blighting with filter paper prior to each weighing. The degradation valuations were achieved as defined by Zhu et al(Zhu et al., 2013).

2.5. Statistical analysis

Statistical analysis was performed using a one-way analysis of variance (ANOVA) in Excel 2016 with significance set at $p < 0.05$. All statistical values were reported as means of standard deviation.

3. Results

3.1. Factors to control CME/N66 fiber formation

To study the fiber morphology of any of the components in core and shell individually, a typical single needle as spinneret was applied to spin the materials. As shown in Fig. 2a-d, fiber morphologies are quite uniform with no bead formation. To determine the relative degree of fiber alignment, FFT analysis on the SEM images was performed, Fig. 2e-h. A randomly oriented fiber sample displays a radially diffuse image in FFT analysis, whereas a highly aligned fiber sample shows a high intensity line normal to the fiber orientation. The FFT images were then analyzed in directionality profile, wherein the radial intensity was summed and plotted with regards to the angle of orientation. As shown in Fig. 2e and g, the fibers produced from N66 were least aligned. The fibers formed from CME applying the same process parameters, had a narrow peak, with the small area under the curve. Higher fiber diameter and higher orientation were observed in the nanofibers from CME, indicating higher chain entanglement.

Table 1 reveals the controlled process parameters and observations in two sections of the typical electrospinning and the coaxial electrospinning to understand the component response when both solutions were supplied simultaneously to the coaxial needle.

In the case of coaxial electrospinning, it was observed that by applying less than 10 kV voltage, yellowish fibers were formed on the collector, whilst pink droplets in core were dropping. Afterwards, by increasing the applied voltage, the pink solution of polar polymer (N66) was electrostatically initiated to orient towards the collector when associated dipole polarization occurred. Hence, the color of the fibers altered from pinkish yellow to a yellowish pink by increasing the intensity of the electrical field. This response to the variable intensity of the electric field, can be deliberated as an observable variation in the core shell fiber composition. In voltages above 20 kV, a pinkish 2D nonwoven mat was gradually fabricated over the collector.

Thus, to understand the effect of the intensity of the electric field on the electrospun fiber composition by coaxial electrospinning, we studied three samples that were obtained from the following voltages: 8 kV (S1P5), 12 kV(S2P5) and 16 kV (S3P5). Then the properties of core-shell structure of nanofibers were investigated. Fig. 3 shows the SEM micrographs and the associated fiber diameter scattering of the electrospun fibers at the studied voltages. It can be seen that the average fiber diameter significantly increased by increasing the electric field, approximately from 1876 nm to 5951 nm. The studied samples showed a narrow peak and were mostly similar to CME nanofibers in orientation.

We used CIE00 color difference as an evidence of hue difference of samples (ΔH) as shown in Table 2. The differences in brightness of samples were eliminated during the calculation due to the size dependency of this value. It can be seen from ΔH values that the hue differences in $\Delta H2$ is significantly lower in value than those in $\Delta H1$. This can be addressed by considering the mechanism of core shell fiber formation in the following discussion section.

Table 2
CIE DE 2000 hue difference between the references and samples

Sample	ΔH_1 [a)]	ΔH_2 [b)]
S1P5	30.521	17.281
S2P5	33.655	17.272
S3P5	38.802	12.912
N66	124.108	0
CME	0	124.108

a) The LAB coordinates of CME were used as the reference color
b) The LAB coordinates of Nylon 66 were used as the reference color

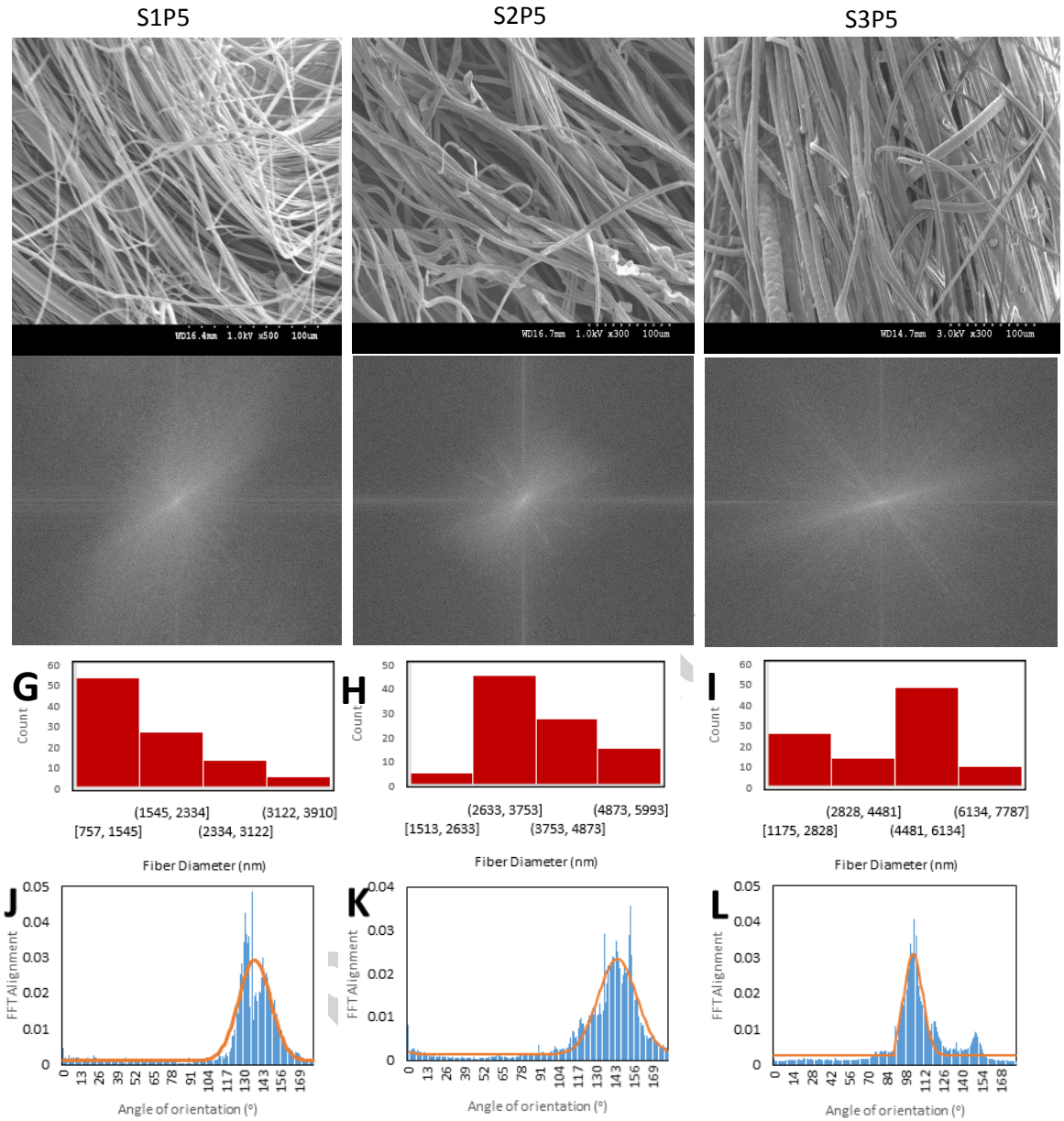

Fig. 3 The effect of applied voltage on the mean fiber diameter and the uniformity of the core-shell fibers (standard deviation value) and the alignment of the core-shell nanofibers of coaxial electrospinning from ASC-g-P(MMA-co-EA) and Nylon 66: S1P5, 8 kV (A, D, G, J); b) S2P5, 12kV (B, E, H, K); S3P5, 16 kV (C, F, I, L). (A- C) SEM images of ASC-g-P(MMA-co-EA)/ Nylon 66 the core-shell nanofibers collected by a rotating drum with constant rotary speed of 423 rpm. (D- F) Image J Raw output of the 2-D FFT alignment analysis of core-shell nanofibers corresponding to SEM images in (A- C); (G- I) fiber diameter frequency plots; (J -L) directionality histogram plots reporting 2D-FFT alignment based on peak shape and the relative principle axis of orientation for the core-shell nanofibers.

3.2. Yarn modulus and tenacity

The mechanical properties of twisted yarns from electrospun nanofibers and core-shell nanofibers from coaxial electrospinning were investigated. Fig. 4 shows the tensile stress/strain relationship of the twisted fiber yarn tested by the Instron tensile testing apparatus following the yarn tensile testing standard (BS-EN-ISO 2062:2009). The fiber yarn samples were prepared with the same linear density using ASTM D5344- 99(2017). For each sample, five specimens were prepared. Each specimen was held between the jaws of the Instron Tensile Tester applying load until breaking, wherein their two ends were fixed by a paper frame, Fig. 4a. The above mentioned samples were then compared with the nanofibers from the core and the shell components that were electrospun individually; electrospun nanofibers of CME and electrospun nanofibers of N66 were studied as reference. Modulus and tenacity were calculated for each specimen by software; by dividing the load (N) to yarn linear density (Tex). And the mean and standard deviation values were calculated for each group of specimens (n=5) referring to initial modulus and tenacity of the samples Table 3, referring to stiffness and strength of the samples, respectively. Modulus represents their resistance to deformation. This measurement was performed as the ratio of tenacity to strain, wherein the tenacity was calculated based on breaking force divided by the initial linear density of the samples, representing the mass stress at break.

According to Table 3, a significant enhancement was observed in the studied samples in contrast to those nanofibers obtained from the core (N66) and the shell (CME) individually. Necking occurred beyond the yielding point in S2P5 and S3P5. Thereafter, elongation progressed to reach breaking extension. This behavior was not observed in S1P5. S1P5 showed that it was brittle in terms of lower breaking stress at a lower elongation by contrast with S2P5 and S3P5 that were fabricated in higher electric field intensity.

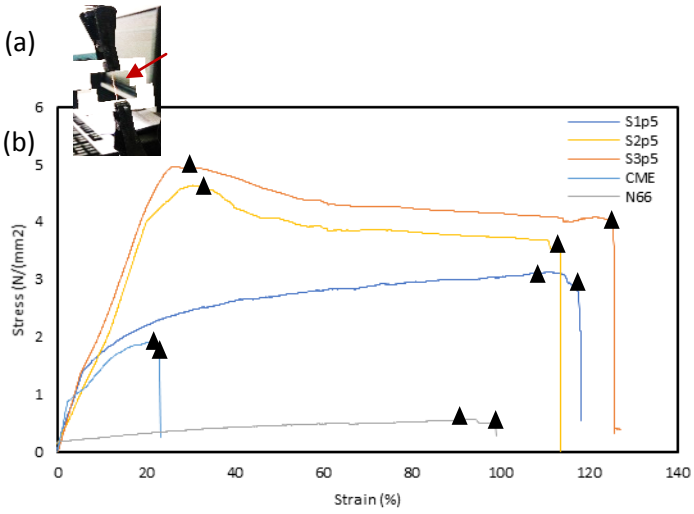

3.3. Thermal behavior of Coaxial Composite Nanofibers

The results of the heat flow versus temperature of CME, N66 and the studied samples are shown in Fig. 5a. The samples were analyzed from 23°C to above the melting temperature (T_m)of N66 (300℃) at a rate of 10 °C min^{-1}. The melting curves were also shown with the same scaling, but were displaced in the same graph for clarity. The DSC curve of CME demonstrates an endothermic peak (downward) at 57.2 °C and 152 °C associated with Tm of the ASC segment and Tm of PMMA, respectively. As denaturation process temperature (Td) of ASC was expected in the melting region of PMMA, the second endothermic peak is contributed to Td of the ASC segment as affected by Tm of PMMA. The glass transition temperature (T_g) and T_m of the N66 are commonly reported at 57°C and 265℃. Due to the size-dependent T_g and T_m of the electrospun N66 fibers, a significant decrease in mentioned temperatures was observed.

Table 3
Mechanical properties of samples

Samples	Breaking Stress (N/mm2)[a)]	Breaking Strain (mm/mm)[a)]	Tensile Stress (N/mm2)[b)]	Tensile Strain (mm/mm)[c)]	Tenacity (cN/Tex)[b)]	Modules (cN/Tex)[b)]
S1P5	2.75± 0.29	1.17± 0.12	3.14± 0.13	1.14± 0.29	5.53± 0.29	21.33± 1.92
S2P5	3.54± 0.71	1.13± 0.21	4.52± 0.27	0.30± 1.40	1.57± 1.40	110.52± 3.14
S3p5	4.01± 0.36	1.25± 0.11	4.86± 0.33	0.29± 0.16	15.29± 0.16	104.75± 6.02
CME	1.77± 0.17	0.22± 0.02	1.93± 0.10	0.21± 0.03	25.30± 0.03	25.58± 2.41

a) (p= 0.001)
b) (p< 0.01)
c) (p < 0.003)

Due to the varied thermal performance of the CME and N66 coaxial composite, we analyzed the impact of CME on the well-known thermal behavior of N66. According to Fig. 5a and Table 4, the nanofibers of N66 demonstrated reduced T_g at 55°C and two peaks of 256.6 °C and 259.8°C in the melting region. Interestingly, an endothermic peak of CME was observed at 57.4°C in S1P5 while this peak cannot be observed in S2P5 and S3P5. Above 250°C, multiple melting peaks were detected in all CME/N66 samples. The minor melting peak (T_{m1}), is attributable to the melting of the original chain arrangement (crystals) of N66 in the fibers. The higher melting peaks (T_{m2}) were caused by the melting of crystals that either re-crystallized or reorganized in heating after melting of the original chain arrangement. T_{m1} and T_{m2} of all samples were shifted to a lower temperature, as shown in Table 4.

Another explanation for the interaction of CME/N66 can be the heightening of N66 crystals in contrast with that observed in N66 fibers (6.99%). This value was obtained from the area of the crystallization exothermic event in cooling. The crystallinity (C%) of N66 in the samples is shown in the last column of Table 4. While C% was decreased in S1P5, an increase was observed in S2P5 and S3P5. The DSC results of CME/N66 fibers in cooling are shown in Fig. 5b. The crystallization temperature of CME/N66 fibers slightly decreased with the exemption of S1P5.

Fig. 4 A typical stress strain curve recorded from tensile test of fiber yarns; Tensile strength point and Breaking point displaying with black marks on curves.

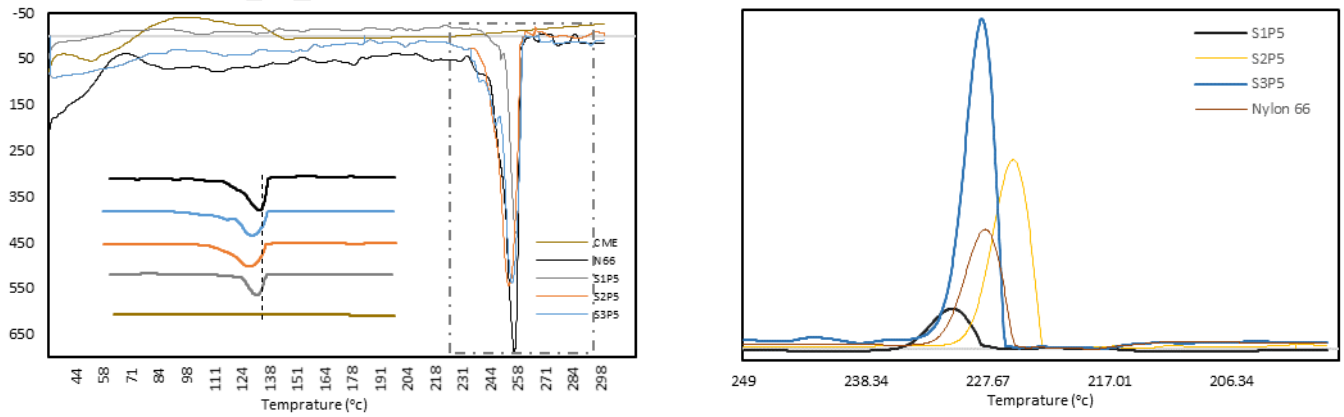

Fig. 5 a) Heat flow vs. temperature of nanofibers, in DSC heating phase with the rate of 10°C min^{-1} in aluminum pan. To clarify, curves associated with the melting region of Nylon 66 were demonstrated vertically in the same graph. b) Dev. Heat flow vs. temperature of nanofibers, during DSC cooling phase from the melt with the rate of 10°C min^{-1}.

Table 4
Melting and crystallization temperatures of samples

Samples	Tm_1 (°C)	Tm_2 (°C)	Tc(°C)	C%
N66	256.61	259.81	228.63	6.99
S1P5	250.66	258.14	231.11	5.78
S2P5	256.41	257.22	226.84	10.91
S3P5	257.02	257.96	229.71	19.06
CME	57.25	152.01	-	-

3.4. Surface wettability, water absorption and degradation properties of the electrospun fibers

Fig. 6a shows the water contact angles (Water CAs) of CME/N66 nonwoven fibrous mats. The water CAs decreased in all samples from 54.62° to 69.18° in the first 10 seconds, while that of the CME and N66 fibers showed the value of 65.80° and 76.07° respectively. The water CA analysis of CME/N66 indicates high surface wettability. However, the water CA of N66 showed a significant decrease after 10 minutes that is not comparable with CME and CME/N66 fiber samples, Fig. 6b. This is due to the high polarity of the N66 that causes the droplet to penetrate through the fiber porous structure, while the samples inherited their surface behavior from CME. These results are in a good agreement with the hydration degree (water absorption) measured after 12 hours, where the initial weight of CME achieved a 44.20% growth and the samples showed a value between the water absorptions of N66 and CME, Fig. 6c.

As shown in Fig. 6c, t(0) value indicates the water uptake of samples in the first moment when were soaked in water, which was calculated in percentage based on added weight, and t(12) based on the added weight after 12 hours into t(0) value divided by the whole weight at t(0). The final water absorption was considered by adding the percentage of t(0) and t(12). Hydration degree of the studied fibers did not exceed 15 g.g-1% with significantly reduced water penetration according to the contact angle studies. From the incubation in PBS for 5 weeks (Fig. 6d), it is found that all core shell samples presented a postponed starting point of degradation. Interestingly, from mass residual percentage observations, when CME was found a significant decrease to 95% during the second and third week, the ASC degradation was started after about 4 weeks in CME/N66 core shell composite nanofibers.

4. Discussion

4.1. Synthesis of ASC-g-P(MMA-co-EA)

ASC is a conversion of collagen involving broken hydrogen bonds and partially broken covalent interchain bonds with a random coil conformation (Abbah et al., 2015; Freed et al., 1994).
One pot approach was applied to solubilizing the collagen chain followed by free radical graft polymerization of MMA-co-EA onto ASC. This was done to significantly reduce the hydrophilicity of the polymer chain of collagen. Details of the synthesis of the graft copolymers have been reported in our previous work (Bazrafshan and Stylios, 2017) in which the side branched hydrophilic copolymer, ASC-g-P(MMA-co-EA) (CME), significantly influenced the initial viscosity in the studied feed ratios of the co-monomer and demonstrated the meaningful reduction of the conductivity value, where the side chain copolymer with the low dielectric constant covalently bonded onto the collagen. In the current research, we used CME as mentioned in the experimental section to evaluate the handling of the fiber formation through electrospinning.

4.2. Assembly mechanism of core shell fibers

We hypothesized that (i) the coaxial electrospinning can provide the possibility to process both components in core and shell simultaneously in which they are unlikely to spin through conventional spinning methods such as melt spinning and wet spinning, or through blending systems; (ii) the polarization of the polymers in core and shell with varied capacity of built-in dipoles is dependent on intensity of the applied electric field, i.e. the fluids in core and shell can move and orientate freely when they are placed in an electrical field. However, it is possible to have a limited region in intensity of the electric field that allows both components to form a single fiber by coaxial electrospinning; (iii) consequently, varied fiber compositions can be fabricated due to increasing the intensity of the electric field within that region.

It is well noticed that N66 possesses a greater dielectric constant in contrast to P(MMA-co-EA) that is settled as the side chain of ASC. Furthermore ASC is a polyelectrolyte (Bhardwaj and Kundu, 2010; Wang et al., 2014), but the dielectric properties of P(MMA-co-EA) in the side chain of ASC is more likely to be overcome vigorously due to electrostatic induction and polarization(Bazrafshan and Stylios, 2017). Then, a higher polarization orientation can occur by a larger factor of the dielectric constant under the influence of the electric field (Kuo et al., 2008; Lee et al., 2011; Rao et al., 2002; Yousefi et al., 2014).

Hence, we used the same solvent for any components in the core and the shell to eliminate the influence of the medium. Additionally, other solution and process parameters were constantly controlled to study the influence of intensity of the electric field

on tuning the fiber properties in all achieved fiber compositions. To understand the behavior of these two incompatible polymers in structure and electrical properties, we used dyes with no overlay in color which allowed us to distinguish the fabricated fibers by color changing. And to understand varied dielectric polarization of the core and the shell components, a negatively charged rod was placed close to the edge of the fibers obtained from each component, CME and N66, individually. It was observed that the negatively charged rod repelled the non-woven mat from CME and attracted the edge of N66 nanofibers.

As shown in Table 1, there was a limited region in the strengthening electrical field that allowed both components; the core and the shell to make a single fiber while stretching towards the collector. Hence, it can be explained that by means of increasing voltage, a significant varied orientation in core and shell components happens when they are exposed to the field. And due to different polarization dimensions of materials in core and shell, a specific region of strengthening electrical field can initiate built-in dipoles of both components to fabricate a single fiber that would lead the whole spun fibers towards the minimum of the dipole energy in a partially ordered shape of deposition.

In other words, by increasing the voltage, one particular moment in time when a certain electrostatic force is reached; N66 in core (red) is to accompany the shell component (CME, yellow) which is already initiated in a low electric field intensity, Table 1. And the shell polymer is influenced by the impulsion of the dipoles that are oriented by N66 due to the effect of the greater

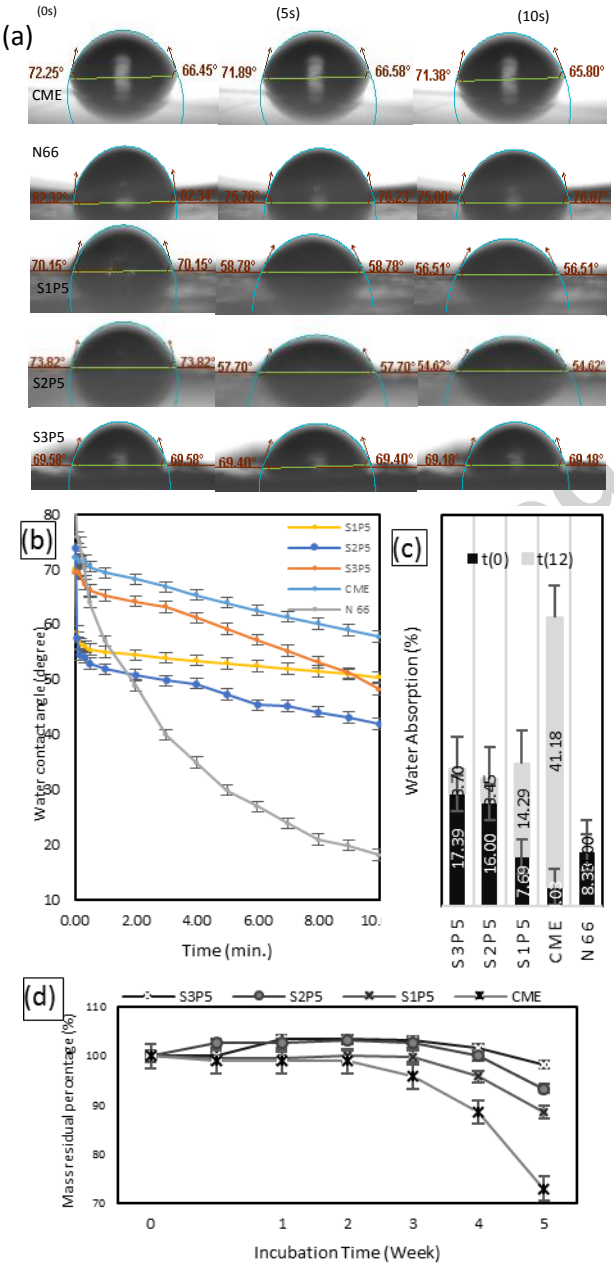

Fig. 6 The water contact angle vs. time: a) 10 seconds, b) 10 minutes; c) Water absorption (hydration degree) of the samples in percentage, d) Mass residual percentage vs. incubation time (week)

polarization orientation into the strengthened electric field. By further increasing the intensity of the electric field, increasing orientation of N66 can be achieved; as shown by the stronger color of N66, Fig. 1(6). It is also possible that the branched copolymer of CME provides sufficient entanglement to form the continuous fibers which can act as a preventive scaffold for stretching N66 in the core. This phenomenon enabled aligned fibers on the axis of drum rotation in voltages between 8-16 kV. This explanation is in a good agreement with the increase in the mean fiber diameter by increasing the applied voltage from 8 to 16 kV which was observed in S1P5 to S3P5 samples, Fig. 3. This was also apparent in the hue differences when the LAB coordinates of N66 were used as the reference color, Table 2.

4.3. FTIR study and Thermal Analysis of the electrospun fibers

To study the interaction between N66 and CME chains, FTIR and DSC were applied. The main characteristic features of the processed samples were observed in the spectra, Fig. 7. ASC has several characteristic absorption bands known as amide A (3425 cm^{-1}), amide B (2857-2953 cm^{-1}), amide I (1615-1711 cm^{-1}), and amide II 1446 cm^{-1} in the infrared region of the spectrum(Li et al., 2013). Characteristic bands of P(MMA-co-EA) were carbonyl (C=O) stretching vibration at 1720 cm^{-1}, CH stretching vibration at (2900-2970 cm-1) and 2865 cm^{-1}, C-O-C stretching at 1060 cm^{-1}, and C-O-C stretching at 1260 cm^{-1}. The amide I adsorption that originated largely from the C=O stretching vibration, is specifically sensitive to the secondary structure of the polypeptides (Pielesz, 2014). For the amide B, the amide II region is affected by P(MMA-co-EA) absorptions, the amide A band and amide I were used as the reference peaks to confirm the presence of Collagen in CME. This helped to study the interaction between CME and N66 in fibers.

For CME fibers, the Amide I peak at 1625 cm^{-1} is assigned to the shift from 1655 to 1625 cm^{-1} that can be caused by β-sheet conformation in contrast with the random-coil backbone conformation (1655 cm-1) (Aluigi et al., 2008; Chen et al., 2008). For CME/N66 fibers cast from KBR, apparent peaks can be observed at 1628, 1612, 1618cm–1 (S3P5, S2P5, S1P5 respectively), indicating that β-sheet secondary structures (i.e., parallel chains, chain orientation) were formed in either CME or CME/N66 fibers. Furthermore, due to the N-H stretching vibration, the amide A does not depend on the conformation but is very sensitive to the strength of a hydrogen bond. When the Amid A of CME observed in 3421 cm^{-1}, it was shifted to higher wavelengths of about 3415, 3383,3361 in all the samples (S1P5- S3P5). However, the amide A peak of N66 improved from 3302 cm^{-1} to 3320,3305,3307 in all samples from S1P5 to S3P5 respectively.

In CME/N66 fibers, the Amide II peak of N66 (1542 cm^{-1}) are still available at the new absorption bands at 1551, 1551,1563 cm^{-1} (S3P5, S2P5 and S1P5, respectively) are causing a new vibration of C=O stretching in the CME/N66 fibers which cannot be distinguished simply in CME due to interaction between ASC chain and P(MMA-co-EA). These band alternations can be related to the interaction between N66 and CME backbone chains. This can be explained by some hydrogen bonds that may be shaped between CME and N66 chains. The presence of new hydrogen bonds between CME and N66 will affect the vibrations of the C=O bonds and they can be seen as a change in Amide A, I and II regions.

Since the CME chain was affected by the interaction of ASC and P(MMA-co-EA), it is difficult to discuss the interaction between CME and N66 in the Amide II absorbance bands. The same situation arises with the Amide III region, as observed in all samples at 1366 cm^{-1}.

Typically, it is believed that a strong interaction between the components of a material can alter the thermal stability of the whole system(Chen et al., 2008). The altered thermal performances of the CME/N66 coaxial fibers are important due to two main reasons. The core-shell structure of the fibers is beneficial for the performance of the CME segment in heat transfer efficiency compared with the nanofibers from pure ASC-g-P(MMA-co-EA). This unique tunable core-shell structure of coaxial nanofibers showed improved thermal stability than the electrospun nanofibers from any individual component. The DSC curves in the cooling phase indicated that the maximum crystallinity percentage of coaxial nanofibers was much higher than that of pure electrospun N66 nanofibers. The crystallinity percentage of S3P5 nanofibers was about three times higher than that of pure N66 nanofibers. And this can be due to a firmly interconnected network, e.g. hydrogen bonding, that was formed during electrospinning between CME and N66.

This investigation was continued with a study of the mechanical effects of the tunable core-shell composite structure of coaxial nanofibers using a mechanical load/extension test with statistical characterization. This enabled a measurable comparison between the core-shell components individually and the core-shell fibers of coaxial electrospinning, as shown in a representative tensile stress-strain curve, Fig. 4. According to Table 3, the tensile characteristics of the electrospun nanofibers from any individual component are far lower than the core-shell structure of coaxial electrospinning with the exemption of young's module of CME,

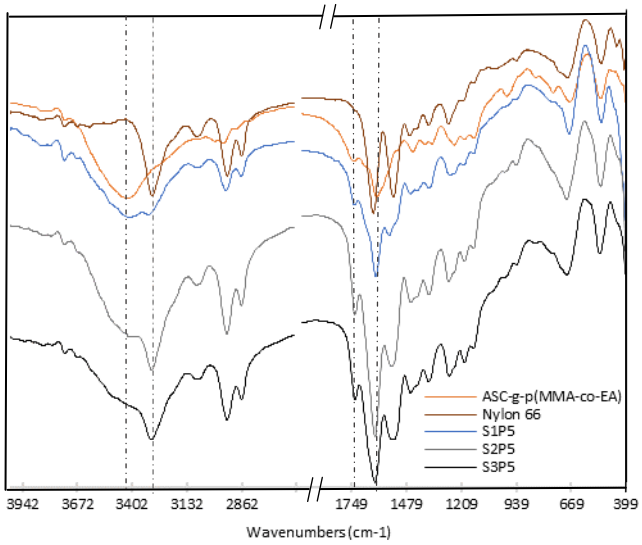

Fig. 7 FTIR Transmittance vs. frequency for samples

which showed a higher stiffness than S1P5.

It is often reported that reducing in fiber diameter can significantly enhance the mechanical properties of electrospun fibers, in typical electrospinning (Bhardwaj and Kundu, 2010; Huang et al., 2004; Kwon et al., 2005) and also several studies have shown that nanofibers with high alignment exhibit remarkable advantages in terms of their mechanical properties(Chen et al., 2009; De Pra et al., 2017; Kharaziha et al., 2013; Yan et al., 2012). We found an increase in fiber diameter and also partial fiber alignment in the studied samples of the CME/N66 composite coaxial fibers along with the reinforcement of their mechanical performances. The reinforced mechanical performance of the CME/N66 composite coaxial nanofibers is benefitted from the branched structure of the CME segments due to increasing stress transfer efficiency. By comparing the mechanical performance and the morphologies of the individual components of nanofibers, we can say that the morphology cannot be the only reason for this enhancement. But it is rather the synergy of a variety of factors that affect the composite nanofiber from the mechanical point of view. Among them, the dipole-dipole interactions of components in the CME/N66 core shell composite fibers, e.g. hydrogen bonding is highlighted as a key factor for stress transfer. Also chain entanglement within the fibers can rely on intermolecular interactions. Additionally, the intrinsic stiffness of the branched CME and a possible rod-like orientation of N66 within the nanofiber structure can increase the mechanical performance of the core-shell composite fibers. Therefore, due to the strong intermolecular interactions, the fiber samples not only achieved the chain orientation but also a significant enhancement was observed in mechanical properties.

1. Conclusions

Due to diverse applications of hydrophilic fibrous assemblies and their ever increasing demand of multi-functional properties, we investigated a new approach using incompatible polymers for the formation of a composite fiber with enhanced chemical and mechanical properties. We synthesized Acid Soluble Collagen-g-P(methyl methacrylate-co-Ethyl Acrylate) (CME). CME was electrospun simultaneously with Nylon 66 (N66) by coaxial electrospinning as a composite that are unlikely to be spun through conventional spinning methods otherwise. The capacity of built-in dipoles of the components in the core (N66) and the shell (CME) with varied electrical properties is dependent on the intensity of the applied electric field. Varied fiber compositions were achieved by increasing the applied voltage. The fiber samples achieved tunable properties from the core and the shell components. We found an increase in fiber diameter and also partial fiber alignment in the studied samples of the CME/N66 coaxial fibers along with reinforcement of their mechanical performances. This enhancement is due to the dipole-dipole interactions of components in the CME/N66 core shell composite fibers, e.g. hydrogen bonding. The studied samples displayed different thermal behavior as well as surface wettability, water absorption and degradation properties, due to varied material compositions. The consequence of this work is that natural-based polymers can be modified to achieve multiple end-uses, not restricted to biomedical, but expand to technical and high performance applications.

References

Abbah, S.A., Delgado, L.M., Azeem, A., Fuller, K., Shologu, N., Keeney, M., Biggs, M.J., Pandit, A., Zeugolis, D.I., 2015. Harnessing Hierarchical Nano- and Micro-Fabrication Technologies for Musculoskeletal Tissue Engineering. Advanced Healthcare Materials 4, 2488-2499.

Aluigi, A., Vineis, C., Varesano, A., Mazzuchetti, G., Ferrero, F., Tonin, C., 2008. Structure and properties of keratin/PEO blend nanofibres. European Polymer Journal 44, 2465-2475.

Averous, L., Pollet, E., 2011. Biorenewable nanocomposites. M R S Bulletin 36, 703-710.

Bazrafshan, Z., Stylios, G.K., 2017. One-pot approach synthesizing and characterization of random copolymerization of ethyl acrylate-co-methyl methacrylate with broad range of glass transition temperature onto collagen: One-Pot Approach Synthesizing and Characterization of Random Copolymerization of Ethyl Acrylate-co-Methyl Methacrylate With Broad Range of Glass Trans. Polymer Engineering & Science.

Bhardwaj, N., Kundu, S.C., 2010. Electrospinning: A fascinating fiber fabrication technique. Biotechnology Advances 28, 325-347.

Bhattacharya, A., Misra, B.N., 2004. Grafting: a versatile means to modify polymers - Techniques, factors and applications. Progress in Polymer Science 29, 767-814.

Bhuiyan, D., Jablonsky, M.J., Kolesov, I., Middleton, J., Wick, T.M., Tannenbaum, R., 2015. Novel synthesis and characterization of a collagen-based biopolymer initiated by hydroxyapatite nanoparticles. Acta Biomaterialia 15, 181-190.

Bledzki, A.K., Gassan, J., 1999. Composites reinforced with cellulose based fibres. Progress in Polymer Science 24, 221-274.

Chen, F., Su, Y., Mo, X., He, C., Wang, H., Ikada, Y., 2009. Biocompatibility, Alignment Degree and Mechanical Properties of an Electrospun Chitosan–P(LLA-CL) Fibrous Scaffold. Journal of Biomaterials Science, Polymer Edition 20, 2117-2128.

Chen, H., Hu, X., Cebe, P., 2008. Thermal properties and phase transitions in blends of Nylon-6 with silk fibroin. Journal of Thermal Analysis and Calorimetry 93, 201-206.

Correia, T.R., Ferreira, P., Vaz, R., Alves, P., Figueiredo, M.M., Correia, I.J., Coimbra, P., 2016. Development of UV cross-linked gelatin coated electrospun poly(caprolactone) fibrous scaffolds for tissue engineering. International Journal of Biological Macromolecules 93, 1539-1548.

Cross, V.L., Zheng, Y., Choi, N.W., Verbridge, S.S., Sutermaster, B.A., Bonassar, L.J., Fischbach, C., Stroock, A.D., 2010. Dense type I collagen matrices that support cellular remodeling and microfabrication for studies of tumor angiogenesis and vasculogenesis in vitro. Biomaterials 31, 8596-8607.

De Pra, M.A.A., Ribeiro-do-Valle, R.M., Maraschin, M., Veleirinho, B., 2017. Effect of collector design on the morphological properties of polycaprolactone electrospun fibers. Materials Letters 193, 154-157.

Freed, L.E., Vunjaknovakovic, G., Biron, R.J., Eagles, D.B., Lesnoy, D.C., Barlow, S.K., Langer, R., 1994. BIODEGRADABLE POLYMER SCAFFOLDS FOR TISSUE ENGINEERING. Bio-Technology 12, 689-693.

Fujisawa, S., Kadoma, Y., 2010. Tri-n-Butylborane/WaterComplex-Mediated Copolymerization of Methyl Methacrylate with Proteinaceous Materials and Proteins: A Review. Polymers 2, 575-595.

Huang, Z.M., Zhang, Y.Z., Ramakrishna, S., Lim, C.T., 2004. Electrospinning and mechanical characterization of gelatin nanofibers. Polymer 45, 5361-5368.

Kaith, B.S., Jindal, R., Maiti, M., 2009. Induction of Chemical and Moisture Resistance in Saccharum spontaneum L Fiber Through Graft Copolymerization with Methyl Methacrylate and Study of Morphological Changes. Journal of Applied Polymer Science 113, 1781-1791.

Kharaziha, M., Fathi, M.H., Edris, H., 2013. Development of novel aligned nanofibrous composite membranes for guided bone regeneration. Journal of the Mechanical Behavior of Biomedical Materials 24, 9-20.

Krissinel, E., Henrick, K., 2007. Inference of macromolecular assemblies from crystalline state. Journal of Molecular Biology 372, 774-797.

Kuo, C.C., Wang, C.T., Chen, W.C., 2008. Highly-Aligned Electrospun Luminescent Nanofibers Prepared from Polyfluorene/PMMA Blends: Fabrication, Morphology, Photophysical Properties and Sensory Applications. Macromolecular Materials and Engineering 293, 999-1008.

Kwon, I.K., Kidoaki, S., Matsuda, T., 2005. Electrospun nano- to microfiber fabrics made of biodegradable copolyesters: structural characteristics, mechanical properties and cell adhesion potential. Biomaterials 26, 3929-3939.

Lee, C.H., Tian, L.M., Abbas, A., Kattumenu, R., Singamaneni, S., 2011. Directed assembly of gold nanorods using aligned electrospun polymer nanofibers for highly efficient SERS substrates. Nanotechnology 22.

Li, M.Y., Mondrinos, M.J., Gandhi, M.R., Ko, F.K., Weiss, A.S., Lelkes, P.I., 2005. Electrospun protein fibers as matrices for tissue engineering. Biomaterials 26, 5999-6008.

Li, W.J., Laurencin, C.T., Caterson, E.J., Tuan, R.S., Ko, F.K., 2002. Electrospun nanofibrous structure: A novel scaffold for tissue engineering. Journal of Biomedical Materials Research 60, 613-621.

Li, Z.R., Wang, B., Chi, C.F., Zhang, Q.H., Gong, Y.D., Tang, J.J., Luo, H.Y., Ding, G.F., 2013. Isolation and characterization of acid soluble collagens and pepsin soluble collagens from the skin and bone of Spanish mackerel (Scomberomorous niphonius). Food Hydrocolloids 31, 103-113.

Mariod, A.A., Adam, H.F., 2013. Review: Gelatin, source, extraction and industrial applications. Acta Scientiarum Polonorum, Technologia Alimentaria 12, 135-147.

Matthews, J.A., Wnek, G.E., Simpson, D.G., Bowlin, G.L., 2002. Electrospinning of collagen nanofibers. Biomacromolecules 3, 232-238.

McKee, M.G., Wilkes, G.L., Colby, R.H., Long, T.E., 2004. Correlations of solution rheology with electrospun fiber formation of linear and branched polyesters. Macromolecules 37, 1760-1767.

Mercader, C., Lucas, A., Derre, A., Zakri, C., Moisan, S., Maugey, M., Poulin, P., 2010. Kinetics of fiber solidification. Proceedings of the National Academy of Sciences of the United States of America 107, 18331-18335.

Pezzoli, D., Cauli, E., Chevallier, P., Farè, S., Mantovani, D., 2017. Biomimetic coating of cross-linked gelatin to improve mechanical and biological properties of electrospun PET: A promising approach for small caliber vascular graft applications. Journal of Biomedical Materials Research Part A 105, 2405-2415.

Pielesz, A., 2014. Temperature-dependent FTIR spectra of collagen and protective effect of partially hydrolysed fucoidan. Spectrochimica Acta Part a-Molecular and Biomolecular Spectroscopy 118, 287-293.

Poormasjedi-Meibod, M.S., Pakyari, M., Jackson, J.K., Salimi Elizei, S., Ghahary, A., 2016. Development of a nanofibrous wound dressing with an antifibrogenic properties in vitro and in vivo model. Journal of Biomedical Materials Research Part A 104, 2334-2344.

Rao, Y., Ogitani, S., Kohl, P., Wong, C.P., 2002. Novel polymer-ceramic nanocomposite based on high dielectric constant epoxy formula for embedded capacitor application. Journal of Applied Polymer Science 83, 1084-1090.

Satyanarayana, K.G., Arizaga, G.G.C., Wypych, F., 2009. Biodegradable composites based on lignocellulosic fibers-An overview. Progress in Polymer Science 34, 982-1021.

Solouk, A., Cousins, B.G., Mirahmadi, F., Mirzadeh, H., Nadoushan, M.R.J., Shokrgozar, M.A., Seifalian, A.M., 2015. Biomimetic modified clinical-grade POSS-PCU nanocomposite polymer for bypass graft applications: A preliminary assessment of endothelial cell adhesion and haemocompatibility. Materials Science & Engineering C-Materials for Biological Applications 46, 400-408.

Song, H.Y., Park, S.J., Hyun, K., 2017. Characterization of Dilution Effect of Semidilute Polymer Solution on Intrinsic Nonlinearity Q(0) via FT Rheology. Macromolecules 50, 6238-6254.

Wang, Q., Yu, D.G., Zhang, L.L., Liu, X.K., Deng, Y.C., Zhao, M., 2017. Electrospun hypromellose-based hydrophilic composites for rapid dissolution of poorly water-soluble drug. Carbohydrate Polymers 174, 617-625.

Wang, Z.L., Cai, N., Dai, Q., Li, C., Hou, D.J., Luo, X.G., Xue, Y.N., Yu, F.Q., 2014. Effect of Thermal Annealing on Mechanical Properties of Polyelectrolyte Complex Nanofiber Membranes. Fibers and Polymers 15, 1406-1413.

Wood-Adams, P.M., Dealy, J.M., deGroot, A.W., Redwine, O.D., 2000. Effect of molecular structure on the linear viscoelastic behavior of polyethylene. Macromolecules 33, 7489-7499.

Yan, J., Qiang, L.H., Gao, Y., Cui, X.J., Zhou, H.Y., Zhong, S.L., Wang, Q., Wang, H.Y., 2012. Effect of fiber alignment in electrospun scaffolds on keratocytes and corneal epithelial cells behavior. Journal of Biomedical Materials Research Part A 100A, 527-535.

Yang, L., Fitie, C.F.C., van der Werf, K.O., Bennink, M.L., Dijkstra, P.J., Feijen, J., 2008. Mechanical properties of single electrospun collagen type I fibers. Biomaterials 29, 955-962.

Yousefi, N., Sun, X.Y., Lin, X.Y., Shen, X., Jia, J.J., Zhang, B., Tang, B.Z., Chan, M.S., Kim, J.K., 2014. Highly Aligned Graphene/Polymer Nanocomposites with Excellent Dielectric Properties for High-Performance Electromagnetic Interference Shielding. Advanced Materials 26, 5480-5487.

Yu, D.G., Li, J.J., Zhang, M., Williams, G.R., 2017. High-quality Janus nanofibers prepared using three-fluid electrospinning. Chemical Communications 53, 4542-4545.

Zeugolis, D.I., Khew, S.T., Yew, E.S.Y., Ekaputra, A.K., Tong, Y.W., Yung, L.Y.L., Hutmacher, D.W., Sheppard, C., Raghunath, M., 2008. Electro-spinning of pure collagen nano-fibres - Just an expensive way to make gelatin? Biomaterials 29, 2293-2305.

Zeugolis, D.I., Paul, R.G., Attenburrow, G., 2009. Extruded Collagen Fibres for Tissue-Engineering Applications: Influence of Collagen Concentration and NaCl Amount. Journal of Biomaterials Science-Polymer Edition 20, 219-234.

Zhu, Y.Q., Hu, C.M., Li, B., Yang, H.L., Cheng, Y.S., Cui, W.G., 2013. A highly flexible paclitaxel-loaded poly(epsilon-caprolactone) electrospun fibrous-membrane-covered stent for benign cardia stricture. Acta Biomaterialia 9, 8328-8336.